Tuning pair-breaking at the surface of topological superfluid ^{3}He

P. J. Heikkinen[1*], A. Casey[1], L. V. Levitin[1], X. Rojas[1], A. Vorontsov[2], P. Sharma[3], N. Zhelev[4], J. M. Parpia[4] and J. Saunders[1]

[1]Department of Physics, Royal Holloway University of London, Egham, Surrey, TW20 0EX, U.K.
[2]Department of Physics, Montana State University, Bozeman, Montana 59717, USA
[3]Department of Physics, Indian Institute of Science, Bangalore 560012, India
[4]Department of Physics, Cornell University, Ithaca, NY 14853, USA

**Corresponding author*: petri.heikkinen@rhul.ac.uk

Since the discovery of superconductivity in heavy fermion metals and oxide materials many emerging superconducting materials have been found to exhibit unconventional, non s-wave, pairing[1]. In contrast to s-wave superconductors, they are extremely sensitive to scattering by non-magnetic defects and surfaces. Topological superfluid ^{3}He, with unconventional p-wave pairing[2-4], provides a model system to understand the influence of surface scattering of quasiparticle excitations in the absence of defect and impurity scattering, which is of relevance to future mesoscopic device applications of topological superconductors[5,6]. Here we confine superfluid ^{3}He within a cavity of height D comparable to the Cooper pair diameter ξ_0. We precisely determine the effect of surface scattering on both the superfluid transition temperature T_c and the suppression of the superfluid energy gap. We demonstrate that the surface scattering can be tuned in situ by adjustment of the isotopic composition of the helium surface boundary layer. In particular we show that suppression of superfluidity is eliminated by a surface coating of thin superfluid ^{4}He film, opening the way to studies of superfluid ^{3}He in the quasi-2D limit[7]. On the other hand, with a magnetic surface boundary layer of solid ^{3}He, an unexpectedly large suppression of T_c is observed, which we model by exchange scattering.

Superfluidity in liquid ^{3}He arises from the formation of spin-triplet Cooper pairs, with one unit ($l = 1$) of orbital angular momentum[2]. The order parameter is a complex 3x3 matrix, encoding the spin state over the spherical Fermi surface. Multiple superfluid phases are therefore possible, all with the same critical temperature T_c. In bulk liquid two phases are found with distinct symmetries[2,3] and momentum-space topologies[4]. The A phase is chiral, breaking time reversal symmetry. Over the Fermi surface pairs form with the same direction of their orbital angular momentum, and in an equal-spin state comprising just $|\uparrow\uparrow\rangle$ and $|\downarrow\downarrow\rangle$ pairs. The B-phase is time-reversal invariant, comprising all three components of the spin triplet, with broken spin-orbit relative symmetry. These two phases provide model systems for topological superconductors, which are the missing "elements" in the periodic table of quantum matter[8]; while candidates exist, no bulk material has yet been unambiguously identified as a topological superconductor[9]. The surface excitations arising from bulk-surface correspondence are not fully protected by topology[4]. Both the density of states of surface excitations and the surface suppression of the order parameter depend on the surface scattering of bulk excitations, quasiparticles which are combinations of particles and holes.

Recently we have shown that it is possible to cool ^{3}He confined within precisely engineered nanoscale cavities into the superfluid phases[10], and detect the nuclear magnetic resonance (NMR) response of the small ^{3}He sample using an ultra-sensitive spectrometer[11]. NMR determines the superfluid transition temperature, the pairing state, and the superfluid energy gap[10,12,13]. The focus of the present study is the understanding and experimental control of surface scattering, which dominates the properties under strong confinement.

The suppression of T_c by non-magnetic impurity scattering has been used to identify non-s-wave superconductivity in a number of materials[14,15]. In superfluid ^{3}He, which is an intrinsically impurity free system, impurities can be artificially introduced using silica-aerogels of different porosities and structure-factor[16]. With homogeneous aerogels there is a linear

suppression $\delta T_c / T_{c0} \sim -\xi_0 / \lambda$ [17,18], where $\delta T_c = T_c - T_{c0}$ is the shift in transition temperature from the pure value, λ is the mean free path for impurity scattering, and $\xi_0 = \hbar v_F / 2\pi k_B T_{c0}$ is the superfluid coherence length, where v_F is the Fermi velocity and T_{c0} the bulk superfluid transition temperature. This is the same dependence as found with both magnetic impurities in s-wave superconductors[19] and non-magnetic impurities in unconventional superconductors[20]. More recently, global anisotropy of the disorder in superfluid ^{3}He has been implemented by nematically ordered[21] or strained aerogels[22]. This has been established to stabilize phases not found in bulk, such as the polar phase[21].

In the work reported here we are able to determine the influence of surface scattering alone on gap suppression, in the absence of impurity scattering, and test the predictions of quasiclassical theory[23,24], for which surface scattering is parameterized by specularity *S*, Fig. 1d, as the single adjustable parameter. Under nanoscale confinement the film thickness is precisely defined by the cavity height *D*, chosen to be comparable to the superfluid coherence length. The effective confinement can be varied at fixed cavity height by changing the sample pressure and hence ξ_0. This contrasts to previous flow measurements on saturated films of different thickness[25-29], where the precise determination of film thickness is difficult.

In our experiment, superfluid ^{3}He was highly confined within a 192 nm high cavity defined in a silicon wafer, Fig. 1a. Measurements were made at a series of pressures from 0 to 5.5 bar, over which ξ_0 decreases from 77 to 40 nm. We determine the shift in the NMR resonance frequency f relative to the Larmor frequency f_L, $\Delta f = f - f_L$, which occurs in the superfluid state. The onset of this shift identifies T_c in the cavity. This is determined precisely relative to the bulk transition temperature T_{c0}, by observing frequency shifts in small volumes of bulk liquid incorporated in the cell design, Fig 1a and Supplementary Figure 1. This measurement is facilitated by the fact that, in the present arrangement, the frequency shifts

from the cavity and the bulk markers are of opposite sign, Fig 1b. The superfluid transition within the cavity is sharp, due to the uniformity of cavity height, relative to that achieved in stacked multiple films with a broad distribution of thickness[30]. The second key piece of information, inferred from the magnitude of the cavity signal frequency shift, is the suppression of the gap by confinement.

The relatively strong confinement in the 192 nm cavity stabilizes the A phase at all temperatures and pressures, consistent with the phase diagram determined in previous work[10,30,31]. The orbital angular momentum of the pairs, which defines the orientation of point nodes of the gap in momentum space, orients normal to the cavity surface $\hat{\mathbf{l}} = \pm\hat{\mathbf{z}}$. The order parameter $\mathbf{\Delta}(\mathbf{p}) = \Delta_{\mathrm{A}}(z)(\hat{p}_x + i\hat{p}_y)\left[\left|\uparrow\uparrow\right\rangle + \left|\downarrow\downarrow\right\rangle\right]$[31], where Δ_{A} is the A-phase gap maximum, which in general has a spatial dependence across the cavity. The static magnetic field $\mathbf{H}_0 = H_0\hat{\mathbf{z}}$ orients the spins along $\hat{\mathbf{z}}$, via the anisotropic magnetic susceptibility. With this relative orientation of spin and orbital angular momentum, the dipolar energy is maximized, accounting for the negative frequency shift observed from the cavity, Fig. 1 (and Supplementary Note 3).

There is compelling evidence that the surface scattering may be tuned *in situ* from diffuse to specular[30,32-35] by coating surfaces with ^{4}He, both from hydrodynamic studies of surface slip[32] in normal state ^{3}He and from transverse acoustic impedance studies[34,35] of surface excitations in ^{3}He-B. These studies are consistent with close to specular scattering in the presence of a superfluid ^{4}He surface film. Quasiclassical theory predicts self-consistently both the surface gap suppression and the suppression of T_c, which for diffuse scattering scales as $\delta T_c / T_{c0} \sim -(\xi_0 / D)^2$ to leading order and which is eliminated for specular scattering. Details of the treatment of surface scattering used in our quasiclassical computations are given in Supplementary Note 2.

We first discuss measurements in which the sample walls and heat exchanger surfaces were plated with sufficient ^{4}He to displace the magnetic solid ^{3}He surface boundary layer, which arises naturally in pure ^{3}He samples[36]. The plating procedure results in a non-magnetic localized solid ^{4}He surface boundary layer. In this case the observed T_c suppression is close to that predicted for purely diffuse scattering. The results are best fit with specularity $S = 0.1$, referred to here as "diffuse", Fig. 2a. The increase in T_c suppression with decreasing pressure arises naturally from stronger effective confinement [31], Fig. 2b. Subsequently a thicker ^{4}He film was formed on the cavity walls to create a surface superfluid film of ^{4}He. In this case we observe an almost complete elimination of T_c suppression, demonstrating close to fully specular scattering, referred to here as "specular", Fig 2a,b.

In general, the measured frequency shift is related to the spatial average of the suppressed gap within the cavity via $\left| f^2 - f_L^2 \right| = \zeta \left\langle \Delta_A^2(z) \right\rangle$, where ζ is an intrinsic material parameter which is pressure dependent but temperature independent (Supplementary Note 3). In the Ginzburg-Landau regime, sufficiently close to T_{c0}, the A-phase bulk gap maximum Δ_A is given by $\Delta_A{}^2 = \frac{\Delta C_A}{C_n}\left(\pi k_B T_{c0}\right)^2 (1 - T/T_{c0})$, where $\Delta C_A / C_n$ is set to the measured heat capacity jump at T_{c0}. This expression thus incorporates strong-coupling corrections to the gap near T_{c0} (Supplementary Note 6). For "specular" boundaries, the measured cavity frequency shift corresponds to the unsuppressed, bulk gap, Fig 2c, and allows determination of the constant ζ at each pressure. For the "diffuse" boundary, using the determined value of ζ, we can precisely infer the gap-suppression from the measured frequency shift, independent of uncertainties in material parameters and temperature scale, Supplementary Note 3. We find the observed gap-suppression is also best described by $S = 0.1$, establishing the consistency of the experimentally determined gap suppression and T_c suppression within the framework of quasiclassical theory.

We now turn to the results where no ^{4}He preplating was deployed, leaving a magnetic surface boundary layer of localized ^{3}He. Rapid exchange with the liquid results in a single hybridized NMR line[30]. The superfluid transition temperature is inferred from analysis of the frequency shift of the hybridized line, which is a weighted average of the internal dipolar frequency shift in the solid ^{3}He surface boundary layer and that due to superfluidity[30] (Supplementary note 6). It shows an unexpectedly large T_c suppression, Fig. 3a, significantly exceeding that observed with a solid ^{4}He boundary layer, and inconsistent with diffuse scattering $S \approx 0$. This result can be *phenomenologically* described in terms of an effective specularity $S_{\text{eff}} = -0.4$. This approaches the condition for maximal pair-breaking $S = -1$, corresponding to full retro-reflection. In this case the phase shift φ experienced by the retro-reflected quasiparticle is $\varphi = \pi$ for all incoming/outgoing trajectories and all surface bound states have zero energy, since $E/\Delta = \pm\cos(\varphi/2)$ [24]. However momentum scattering with a preponderance of retroreflection is inconsistent with measurements of boundary slip in viscous transport in the normal state, which find equivalent specularity ($0 < S < 1$) for both solid ^{3}He and solid ^{4}He surface boundary layers[32].

In the superfluid state the natural candidate to explain the stronger T_c suppression is magnetic surface scattering. In prior work exchange interaction between quasiparticles and isolated impurities has been theoretically established to induce additional bound states in superconductors[37]. Magnetic scattering by localized ^{3}He[38] has been proposed to strongly influence the observed superfluid phase diagram of ^{3}He in nematically ordered aerogel[39], a globally anisotropic medium, while other studies of ^{3}He in aerogel have also been interpreted in terms of an exchange coupling ranging from $J \sim 0.1$ to 0.5 mK[18,40]. In order to explain our result with a magnetic solid ^{3}He surface boundary layer, we seek processes which generate an excess of zero-energy states over that found for diffuse momentum scattering (Fig. 3b and Supplementary Note 7). The structure of the order parameter is such that the phase shift φ

experienced by the scattered quasiparticle, and hence the energy of the surface bound states, will be influenced by spin-dependent scattering processes. We suggest a mechanism in which randomly oriented localized quantum spins, exchange coupled to the incident quasiparticle, give rise to interference between the singlet and triplet scattering channels. We find that this enhances pair-breaking such that, for a surface with momentum scattering specularity S, the suppression of T_c corresponds to an effective specularity between bounds $-S < S_{\mathrm{eff}} < S$, depending on strength of exchange coupling. Thus this process is only detectable for non-diffuse surfaces, but can give rise to T_c suppression exceeding that for a diffuse surface, as observed. In order to reach the detected $S_{\mathrm{eff}} = -0.4$, the required underlying specularity for momentum scattering from the atomically smooth silicon surface with solid ^{3}He surface boundary layer should be $S > 0.4$, which is a plausible scenario (Methods).

In conclusion, we have rigorously tested the validity of quasi-classical theory for non-magnetic boundaries, experimentally demonstrating that it provides a self-consistent description of the suppression of superfluidity at surfaces and under strong confinement. The results with magnetic ^{3}He boundaries motivate further studies of magnetic scattering under different conditions, and the possibility of magnetically-induced effects, such as surface spin currents, and new order parameters under confinement. Precise determination of the gap suppression in the presence of the magnetic surface boundary layer was beyond the scope of this work, since it would require measurements in lower magnetic fields in order to suppress the solid dipolar shift and increase the superfluid frequency shift.

For non-magnetic surfaces, the implications of these results are several. In the case of diffuse scattering, we demonstrate that superfluidity will be completely suppressed in cavities thinner than 100 nm at zero pressure. This opens the door to superfluid devices with normal "leads", Fig. 4, as well as hybrid structures. On the other hand, the demonstration of *in situ* tuning of the surface scattering to close to the specular limit, and the consequent elimination

of both T_c and gap suppression, opens the investigation of cavities of arbitrarily small height towards $D << \xi_0$. As the cavity height is reduced, size quantization along z will play an increasing role and the system will enter the quasi-2D limit, in which thermal and spin analogues of the Quantum Hall effect are predicted[7,41]. In that limit cavity height variations will give rise to an effective disorder potential, already detected in transport measurements over a rough surface[42], and a new theory replacing the picture of surface scattering to reflect the quasi-two-dimensionality will be needed. Overall, the sculpture of the superfluid by confinement opens the new direction of topological mesoscopic superfluidity, with *in situ* tunability through diffuse, specular or magnetic surface scattering.

Methods

Silicon nanofluidic cavity fabrication. The experimental cell was fabricated by direct wafer bonding of two silicon wafers. The confinement region and supporting pillars are defined lithographically on one of the wafers using a process similar to that used in a previous generation of cells[43]. The typical surface roughness of the silicon surface is 0.1 nm[44]. This is significantly smoother than the mechanically polished silicon surfaces for which surface specularity has been characterized by normal state studies of slip in viscous transport[32], potentially promoting specularity of surface scattering even in the absence of a superfluid ^{4}He film. Deep Reactive Ion Etch (DRIE) is used to create two 300 micron diameter holes either side of the confinement region. One acts as a fill line and the other provides a region of bulk helium on the far side of the slab shaped cavity, Fig. 1a. DRIE is also used to pattern the backside of the wafer to improve the joint between the cell and an external fill line[44]. After all the features are patterned onto the wafers they are cleaned using a combination of a two-step RCA clean at 75 °C followed by immersion in concentrated (49%) HF to remove any oxide or contaminants. The clean patterned wafer is brought into contact with a blank silicon wafer within a wafer aligner, forming a bond between the cavity wafer and the lid. The bond strength is increased and made permanent by an annealing step at 1000 °C for 2 hours. Successful bonding is confirmed using infra-red imaging and scanning acoustic microscopy. The bonded wafer is diced into individual cells using a diamond saw. A 500 nm thick silver film is evaporated onto the outside of the bonded wafers to thermalize the cell to the nuclear stage. In order to minimise the effects of differential thermal contraction between the metallic fill line/ far-end bulk marker plug and the silicon cell, laser-machined silicon washers are attached around both of the DRIE holes with epoxy (Stycast 1266 mixed with silicon powder), Supplementary Fig. 1. The height of the cavity used in this work was determined to be 192 nm by a profilometer scan on the unbonded wafer. The error in the cavity thickness ±2nm was estimated from the distribution in height measured in this way across all the cavities on the unbonded wafer. The dependence of cavity height on pressure is determined by finite element method simulations to be 2.6 nm/bar, Supplementary Fig. 2.

NMR measurements. The cooling of the ^{3}He within the cell, the thermometry and the SQUID NMR spectrometer were as used in previous work[10,11], Supplementary Fig. 1. The helium is cooled via the column of ^{3}He in the fill line which connects the cell to a sintered silver heat exchanger mounted on a silver plate, connected via a silver rod to the copper nuclear demagnetization stage. A platinum NMR thermometer is mounted on the silver plate. Measurements were made at a ^{3}He Larmor frequency of 967 kHz, with the static field of around 30 mT applied along the cavity surface normal ($\hat{\mathbf{z}}$). Field gradients were applied to both separate the bulk marker signals from the cavity signal (along $\hat{\mathbf{z}}$), and to resolve the signals from the two bulk markers (along $\hat{\mathbf{x}},\hat{\mathbf{y}}$). The free induction decay following small angle tipping pulses, applied at 10 s intervals, was averaged typically 30 times, and Fourier transformed. Measurements with tipping pulses of different amplitude enabled a correction to be made for temperature gradients between the ^{3}He in the cell and the platinum thermometer (Supplementary Note 1). This correction depended on the surface boundary condition, which influenced the boundary resistance of the silver heat exchanger. The temperature gradient across the cavity is small, and dependent on surface boundary condition; it is determined from the difference between the measured superfluid transition temperature in the two bulk marker volumes. For solid ^{4}He and ^{3}He surface boundary layer the difference is around 20 µK, while for the superfluid ^{4}He surface boundary layer it is at most 2 µK, Supplementary Fig. 10. This gradient is taken into account in determining the error in superfluid transition temperature.

In situ tuning of surface scattering. *Diffuse non-magnetic scattering*. In order to displace the naturally occurring magnetic surface boundary layer of ^{3}He[36], $32\ \mu\mathrm{mol/m^2}$ of ^{4}He was added to the empty cell and silver heat exchanger (surface area 8 m^2) at 30 K, followed by cooling to below 1 K over 30 hours, and a subsequent anneal at 2 K for several hours. This coverage is below that necessary to see a superfluid transition in the surface ^{4}He layer, in the presence of an overburden of ^{3}He at saturated vapour pressure[45]. The sample is cooled to 100 mK before adding ^{3}He. Under these conditions the ^{3}He surface magnetism seen in pure ^{3}He samples is eliminated. *Specular scattering*. To create specular scattering conditions from the previous ^{4}He surface plating conditions, the cell is pumped at 1.5 K, leaving a residual solid ^{4}He "layer" on the surfaces. Then more ^{4}He is added into the cell/heat exchanger. Subsequently the helium pumped out in the previous step is restored. The sample is slowly cooled into the mK range, during which all the ^{4}He forms a surface film of solid ^{4}He with a superfluid ^{4}He overlayer. With nominal surface ^{4}He coverage in the range 68 to $139\ \mu\mathrm{mol/m^2}$, we always detect the same specularity, consistent with previous work[32], which found evidence for surface scattering close to specular for surface film coverages in excess of $60\ \mu\mathrm{mol/m^2}$.

Theoretical calculation of gap suppression is made using quasiclassical theory with the random S-matrix scattering model (Supplementary Note 2).

The error bars in Figures 1 and 2 reflect the upper and lower bounds on the cavity height D, the uncertainty in temperature (Supplementary Note 1), and the standard deviation of the measured superfluid transition temperature. Where error bars are not visible, the relevant error is less than the symbol size.

Data availability. The data that support the plots within this paper and other findings of this study are available from the corresponding author on reasonable request.

Author contributions:

Experimental work was carried out by P.J.H and L.V.L with contributions from A.C. The nanofabricated cells were prepared and assembled by N.Z, X.R and A.C. X.R carried out the FEM simulations of the cell. The analysis and presentation was carried out by P.J.H, L.V.L and A.V with contributions from J.S. A.V performed calculations of gap profile and superfluid transition temperature. A.V developed the theory of magnetic scattering with contributions from P.S. The work at Cornell was supervised by J.M.P, and the work in London was supervised by J.S, A.C and L.V.L, who had the leading roles in formulating the research. P.J.H, J.S and A.V had leading roles in writing the paper, with contributions from all authors.

Acknowledgements:

We thank M. Eschrig, J. A. Sauls, V. V. Dmitriev and A. M. Zimmerman for helpful discussions. This work was supported by EPSRC grants EP/J0220004/1 and EP/R04533X/1, NSF grant DMR-17808341, and the European Union's Horizon 2020 Research and Innovation Programme, under Grant Agreement no. 824109 (European Microkelvin Platform). Fabrication was carried out at the Cornell Nanofabrication Facility (CNF) with assistance and advice from technical staff. CNF is supported in part by the NSF through ECCS-1542081. Measurements were made at the London Low Temperature Laboratory. We thank Richard Elsom, Ian Higgs, Paul Bamford and Harpal Sandhu for technical support.

Competing financial interests: The authors declare no competing financial interests.

Materials & Correspondence: Requests should be addressed to petri.heikkinen@rhul.ac.uk and j.saunders@rhul.ac.uk.

Figure 1.

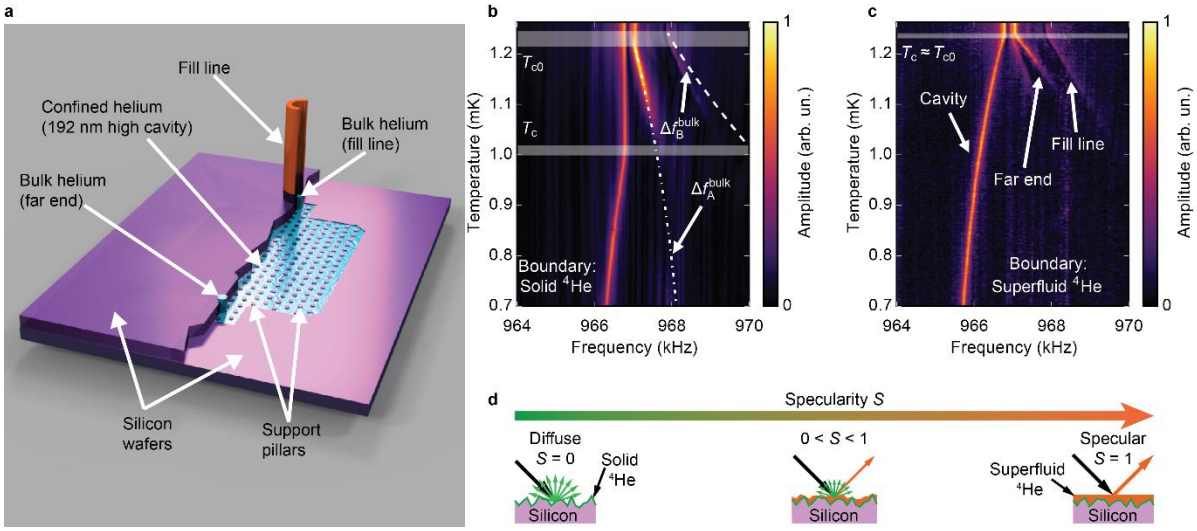

Figure.1 Experimental cell confining ^{3}He. **a**. Nanofabricated sample cell, cut away to show cavity in lower silicon wafer, bonded to upper wafer. The support posts shown maintain cavity height D under different liquid pressures. The cavity is filled through a fill line via a sintered heat exchanger and cooled through the column of ^{3}He within it. Small volumes of bulk liquid at each end of the cavity provide markers for the bulk superfluid transition T_{c0}, and eliminate errors due to temperature gradients. The NMR coil set around the sample is shown in Supplementary Fig. 1. Suitable small magnetic field gradients are used to resolve the NMR response of different regions of the cell, see Methods. **b, c.** NMR signatures of superfluid transition in cavity and bulk markers, for two different surface boundary conditions, at ^{3}He pressure of 2.46 bar. ^{3}He-A in the cavity shows a negative frequency shift whereas the bulk markers show positive frequency shift (Supplementary Note 5). The T_c suppression observed with a surface boundary layer of solid ^{4}He is eliminated by the addition of ^{4}He to create a superfluid ^{4}He film at the surface. **d.** Schematic illustration of the tuning of surface scattering conditions, parameterised by specularity coefficient *S*.

Figure 2.

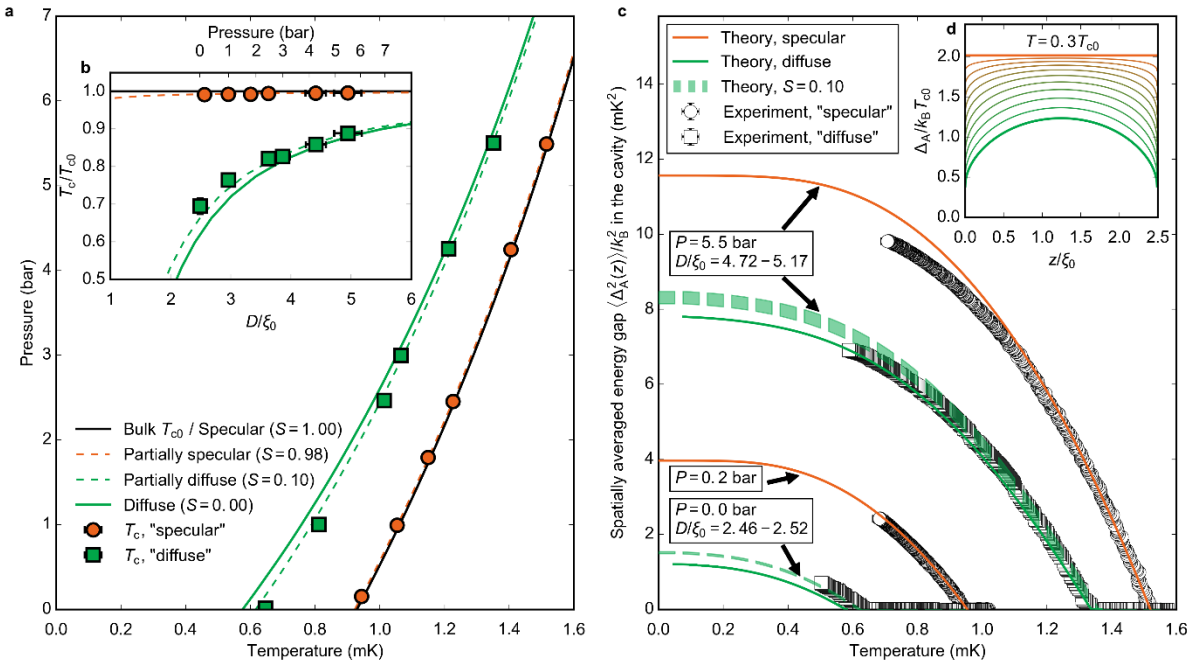

Figure 2. Suppression of superfluid transition temperature and superfluid gap for different surface scattering conditions. **a.** Measured pressure dependence of T_c for close to diffuse and close to specular boundary conditions. Full lines show predicted T_c for diffuse and fully specular boundaries, dashed lines are best fits yielding $S=0.1$ and $S=0.98$. **b**. Suppression of T_c for diffuse boundary steeply increases with confinement. Suppression of T_c for specular boundary is essentially eliminated. **c.** Spatial average of energy gap in cavity at two pressures (0.0, 5.5 bar), inferred from measured frequency shift (Supplementary Note 3), for the two surface scattering conditions studied. At zero bar the "diffuse" experiment agrees best with theory for $S=0.1$, taking into account the weak pressure dependence of cavity height and associated errors (Methods). All theoretical curves include strong coupling corrections valid near T_c. The emergent discrepancy between theory and experiment at lower temperatures at 5.5 bar is in agreement with the expected temperature dependence of strong coupling corrections to the gap (Supplementary Note 4). **d**. The calculated gap profile at zero pressure for specularities between 0 and 1 in intervals of 0.1.

Figure 3.

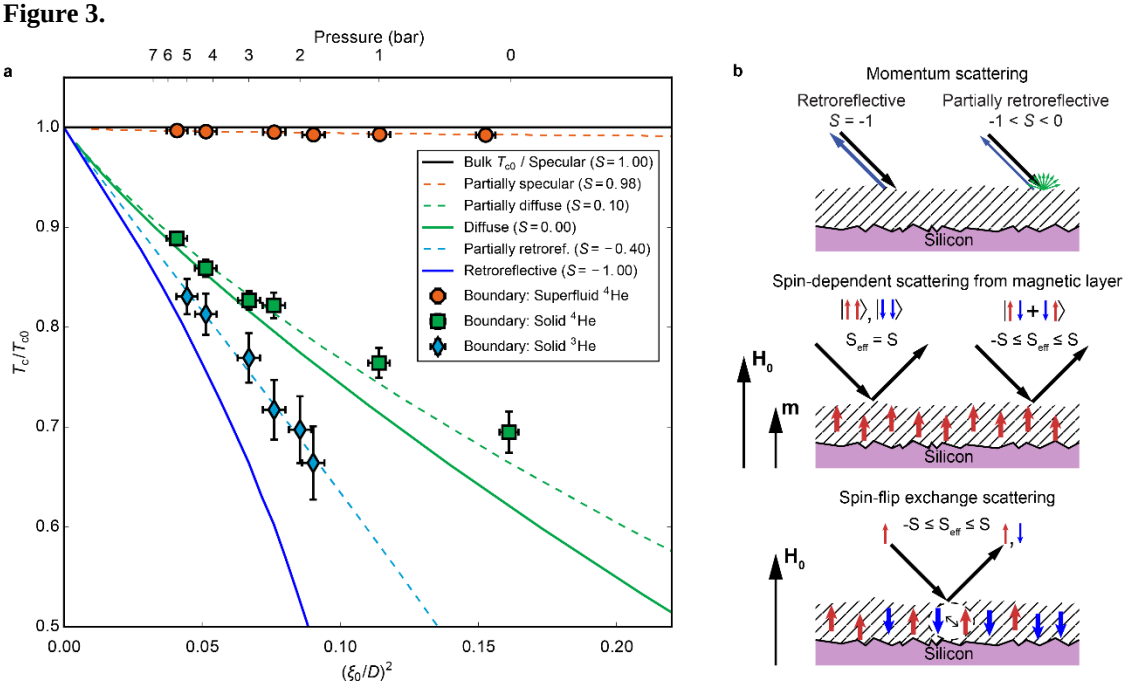

Figure 3.a. Increased suppression of superfluid transition temperature in presence of a magnetic solid ^{3}He surface boundary layer. Plot compares suppression of T_c in cavity relative to that of bulk liquid as a function of square of the inverse effective confinement , where D is cavity height and ξ_0 is the pressure-dependent coherence length, for solid ^{3}He boundary (diamond), solid ^{4}He boundary (square) and superfluid ^{4}He boundary (circles). Full lines show: maximal pair-breaking retro-reflection ($S = -1$); diffuse ($S = 0$); fully specular ($S = 1$). Dashed lines show best fits to the data: $S = -0.4, 0.1, 0.98$. For the solid ^{3}He boundary, T_c is identified from onset of superfluid frequency shift after correcting for background frequency shift arising from magnetic solid layer (Supplementary note 6). **b.** Three candidate scattering mechanisms for negative effective specularity (see also Supplementary Note 7): retroreflection (ruled out by normal state measurements); spin-dependent apair breaking on scattering from a magnetically polarized layer (absent for the relative orientation of surface layer spin polarization **m**, surface normal and spin orientation of A-phase pairs in our set-up); spin-flip exchange scattering (spin-polarization of surface layer can be zero), where the effective specularity S_{eff} is a parameter characterising combined magnetic and momentum scattering, bounded by the specularity S that would arise from momentum scattering alone.

Figure 4.

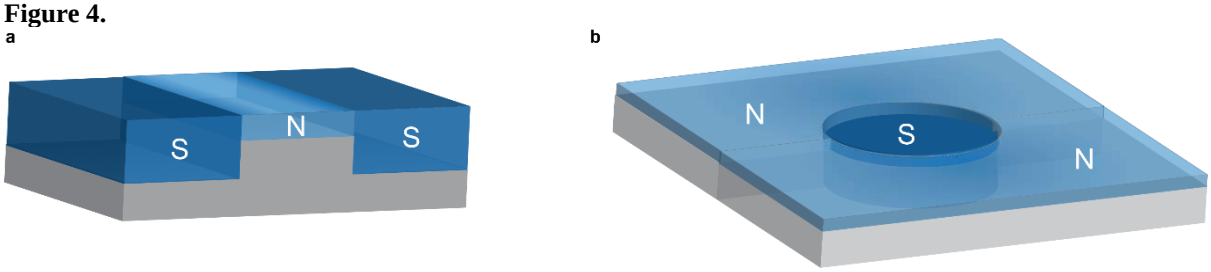

Figure 4. Topological mesoscopic superfluidity. Confinement tunes ^{3}He into different material phases, enabling hybrid structures. **a.** An SNS junction, where spatial modulation of cavity height defines SN interfaces. **b**. Circular region of higher cavity height defines an isolated mesa of superfluid, cooled through normal liquid in a more confined region.

References

1 Norman, M. R. The challenge of unconventional superconductivity. *Science* **332**, 196-200 (2011).

2 Vollhardt, D. & Wölfle, P. *The superfluid phases of helium 3*. (Dover, 2013).

3 Leggett, A. J. A theoretical description of the new phases of liquid 3He. *Reviews of Modern Physics* **47**, 331-414 (1975).

4 Mizushima, T. *et al.* Symmetry-Protected Topological Superfluids and Superconductors-From the Basics to He-3. *Journal of the Physical Society of Japan* **85**, 74 (2016).

5 Anwar, M. S. *et al.* Direct penetration of spin-triplet superconductivity into a ferromagnet in Au/$SrRuO_3$/Sr_2RuO_4 junctions. *Nature Communications* **7**, 13220 (2016).

6 Chung, S. B., Kim, S. K., Lee, K. H. & Tserkovnyak, Y. Cooper-Pair Spin Current in a Strontium Ruthenate Heterostructure. *Phys Rev Lett* **121**, 167001 (2018).

7 Volovik, G. E. *Exotic properties of superfluid ^{3}He*. (World Scientific, 1992).

8 Schnyder, A. P., Ryu, S., Furusaki, A. & Ludwig, A. W. W. Classification of topological insulators and superconductors in three spatial dimensions. *Physical Review B* **78**, 195125 (2008).

9 Sato, M. & Ando, Y. Topological superconductors: a review. *Rep Prog Phys* **80**, 076501 (2017).

10 Levitin, L. V. *et al.* Phase diagram of the topological superfluid ^{3}He confined in a nanoscale slab geometry. *Science* **340**, 841-844 (2013).

11 Levitin, L. V. *et al.* A nuclear magnetic resonance spectrometer for operation around 1MHz with a sub-10-mK noise temperature, based on a two-stage dc superconducting quantum interference device sensor. *Applied Physics Letters* **91**, 262507 (2007).

12 Levitin, L. V. *et al.* Surface-induced order parameter distortion in superfluid ^{3}He-B measured by nonlinear NMR. *Phys Rev Lett* **111**, 235304 (2013).

13 Levitin, L. V. *et al.* Evidence for a Spatially Modulated Superfluid Phase of ^{3}He under Confinement. *Physical Review Letters* **122**, doi:10.1103/PhysRevLett.122.085301 (2019).

14 Mackenzie, A. P. *et al.* Extremely Strong Dependence of Superconductivity on Disorder in Sr_2RuO_4. *Physical Review Letters* **80**, 161-164 (1998).

15 Kycia, J. B. *et al.* Suppression of superconductivity in UPt_3 single crystals. *Physical Review B* **58**, R603-R606 (1998).
16 P. Halperin, W., Choi, H., P. Davis, J. & Pollanen, J. Impurity Effects of Aerogel in Superfluid ^{3}He. *Journal of the Physical Society of Japan* **77**, 111002 (2008).
17 Thuneberg, E. V., Yip, S. K., Fogelström, M. & Sauls, J. A. Models for Superfluid He^3 in Aerogel. *Physical Review Letters* **80**, 2861-2864 (1998).
18 Sauls, J. A. & Sharma, P. Impurity effects on the A1−A2 splitting of superfluid ^{3}He in aerogel. *Physical Review B* **68**, 224502(2003).
19 Abrikosov, A. A. G., L. P. *JETP (USSR)*, 1243 (1961).
20 Larkin, A. I. Vector pairing in superconductors of small dimensions. *JETP (USSR)* **2**, 130-132 (1965).
21 Dmitriev, V. V., Senin, A. A., Soldatov, A. A. & Yudin, A. N. Polar Phase of Superfluid ^{3}He in Anisotropic Aerogel. *Physical Review Letters* **115**,165304 (2015).
22 Li, J. I., Zimmerman, A. M., Pollanen, J., Collett, C. A. & Halperin, W. P. Anisotropic phases of superfluid ^{3}He in compressed aerogel. *Phys Rev Lett* **114**, 105302 (2015).
23 Serene, J. W. & Rainer, D. The quasiclassical approach to superfluid ^{3}He. *Physics Reports* **101**, 221-311 (1983).
24 Vorontsov, A. B. Andreev bound states in superconducting films and confined superfluid ^{3}He. *Philos Trans A Math Phys Eng Sci* **376**, 2015.0144 (2018).
25 Steel, S. C., Harrison, J. P., Zawadzki, P. & Sachrajda, A. ^{3}He film flow on a round rim beaker. *Journal of Low Temperature Physics* **95**, 759-788 (1994).
26 Davis, J. C., Amar, A., Pekola, J. P. & Packard, R. E. Superfluidity of ^{3}He films. *Phys Rev Lett* **60**, 302-304 (1988).
27 Xu, J. & Crooker, B. C. Very Thin Films of He^3 - a New Phase. *Physical Review Letters* **65**, 3005-3008 (1990).
28 Schechter, A. M. R., Simmonds, R. W., Packard, R. E. & Davis, J. C. Observation of 'third sound' in superfluid ^{3}He. *Nature* **396**, 554 (1998).
29 Saitoh, M., Ikegami, H. & Kono, K. Onset of Superfluidity in ^{3}He Films. *Phys Rev Lett* **117**, 205302 (2016).
30 Freeman, M. R. & Richardson, R. C. Size Effects in Superfluid He^3 Films. *Physical Review B* **41**, 11011-11028 (1990).
31 Vorontsov, A. B. & Sauls, J. A. Thermodynamic properties of thin films of superfluid He^3-A. *Physical Review B* **68**, 064508 (2003).
32 Tholen, S. M. & Parpia, J. M. Slip and the effect of ^{4}He at the ^{3}He-silicon interface. *Phys Rev Lett* **67**, 334-337 (1991).
33 Ritchie, D. A., Saunders, J. & Brewer, D. F. Momentum transfer between ^{3}He quasiparticles and surfaces: The effective viscosity of dilute solutions of ^{3}He in ^{4}He. *Phys Rev Lett* **59**, 465-468 (1987).
34 Murakawa, S. *et al.* New Anomaly in the Transverse Acoustic Impedance of Superfluid He^3-B with a Wall Coated by Several Layers of He^4. *Physical Review Letters* **103**, 155301 (2009).
35 Okuda, Y. & Nomura, R. Surface Andreev bound states of superfluid He^3 and Majorana fermions. *Journal of Physics-Condensed Matter* **24**, 343201 (2012).
36 Ahonen, A. I. *et al.* Boundary magnetism in liquid ^{3}He at very low temperatures. *Journal of Physics C: Solid State Physics* **9**, 1665-1672 (1976).
37 Balatsky, A. V., Vekhter, I. & Zhu, J.-X. Impurity-induced states in conventional and unconventional superconductors. *Reviews of Modern Physics* **78**, 373-433 (2006).

38 Mineev, V. P. Influence of exchange scattering on superfluid ^{3}He states in nematic aerogel. *Physical Review B* **98**, 014501 (2018).
39 Dmitriev, V. V., Soldatov, A. A. & Yudin, A. N. Effect of Magnetic Boundary Conditions on Superfluid ^{3}He in Nematic Aerogel. *Phys Rev Lett* **120**, 075301 (2018).
40 Sauls, J. A. & Sharma, P. Theory of heat transport of normal liquid ^{3}He in aerogel. *New Journal of Physics* **12**, 083056 (2010).
41 Volovik, G. E. An analog of the quantum Hall effect in a superfluid ^{3}He film. *JETP (USSR)* **67**, 1084 (1988).
42 Sharma, P. *et al.* Quantum transport in mesoscopic ^{3}He films: experimental study of the interference of bulk and boundary scattering. *Phys Rev Lett* **107**, 196805 (2011).
43 Dimov, S. *et al.* Anodically bonded submicron microfluidic chambers. *Rev Sci Instrum* **81**, 013907 (2010).
44 Zhelev, N. *et al.* Fabrication of microfluidic cavities using Si-to-glass anodic bonding. *Rev Sci Instrum* **89**, 073902 (2018).
45 McQueeney, D., Agnolet, G. & Reppy, J. D. Surface Superfluidity in Dilute ^{4}He-^{3}He Mixtures. *Physical Review Letters* **52**, 1325-1328 (1984).